IJMMM International Journal of Minerals, Metallurgy and Materials 矿物冶金与材料学报（英文版）

Interaction mechanism of cyanide with pyrite during the cyanidation of pyrite and the decyanation of pyrite cyanide residues by chemical oxidation

Wenwen Han, Hongying Yang, and Linlin Tong

Cite this article as:
Wenwen Han, Hongying Yang, and Linlin Tong, Interaction mechanism of cyanide with pyrite during the cyanidation of pyrite and the decyanation of pyrite cyanide residues by chemical oxidation, *Int. J. Miner. Metall. Mater.*, 31(2024), No. 9, pp. 1996-2005. https://doi.org/10.1007/s12613-023-2814-3

INTERNATIONAL JOURNAL OF
Minerals, Metallurgy and Materials

Volume 31, Number 9, September 2024
Page 1996

Research Article https://doi.org/10.1007/s12613-023-2814-3

Interaction mechanism of cyanide with pyrite during the cyanidation of pyrite and the decyanation of pyrite cyanide residues by chemical oxidation

Wenwen Han[1,2], *Hongying Yang*[1,2)✉], *and Linlin Tong*[1,2)]

1) Key Laboratory for Ecological Metallurgy of Multimetallic Mineral (Ministry of Education), Northeastern University, Shenyang 110819, China
2) School of Metallurgy, Northeastern University, Shenyang 110819, China
(Received: 25 June 2023; revised: 21 December 2023; accepted: 22 December 2023)

Abstract: The toxic cyanides in cyanide residues produced from cyanidation process for gold extraction are harmful to the environment. Pyrite is one of the main minerals existing in cyanide residues. In this work, the interaction of cyanide with pyrite and the decyanation of pyrite cyanide residue were analyzed. Results revealed that high pH value, high cyanide concentration, and high pyrite dosage promoted the interaction of cyanide with pyrite. The cyanidation of pyrite was pseudo-second-order with respect to cyanide. The decyanation of pyrite cyanide residue by Na_2SO_3/air oxidation was performed. The cyanide removal efficiency was 83.9% after 1 h of reaction time under the optimal conditions of pH value of 11.2, SO_3^{2-} dosage of 22 mg·g^{-1}, and air flow rate of 1.46 L·min^{-1}. X-ray photoelectron spectroscopy analysis of the pyrite samples showed the formation of Fe(III) and $FeSO_4$ during the cyanidation process. The cyanide that adsorbed on the pyrite surface after cyanidation mainly existed in the forms of free cyanide (CN^-) and ferrocyanide ($Fe(CN)_6^{4-}$), which were effectively removed by Na_2SO_3/air oxidation. During the decyanation process, air intake promoted pyrite oxidation and weakened cyanide adsorption on the pyrite surface. This study has practical significance for gold enterprises aiming to mitigate the environmental impact related to cyanide residues.

Keywords: pyrite; cyanide; decyanation; sodium sulfite/air oxidation; cyanide residue

1. Introduction

A substantial amount of gold cyanide residue is produced during the cyanidation process for gold extraction [1]. The high concentration of highly toxic cyanides in cyanide residues poses a serious threat to the environment and life [2]. Cyanide residues also contain valuable minerals and elements, including precious metals such as gold and silver, as well as iron, copper, and zinc. However, cyanides can adversely affect the flotation of minerals, resulting in low recovery of these valuable elements [3]. Thus, the removal of cyanide in gold cyanide residues must be performed to attain the maximum recovery of valuable resources and render the toxic solid waste innocuous, which has significant economic, environmental, and social benefits.

Iron in gold ores is mainly present as pyrite, a critical gold-bearing mineral [4]. The interaction of cyanide with pyrite influences the properties of gold cyanide residues. It has been reported that cyanides in cyanide residues exist in various forms and can be adsorbed on the surfaces of metallic sulfide minerals such as pyrite, chalcopyrite, and sphalerite [3]. Zhao *et al.* [5] observed that carbon was bonded to one iron atom on the pyrite surface after the adsorption of cyanide ions with an adsorption energy of −327.94 kJ·mol^{-1}. Removal of cyanide on the pyrite surface has a significant effect on the cyanide removal of gold cyanide residues. Therefore, the study on the interaction of cyanide with pyrite and the decyanation of pyrite cyanide residue is helpful in improving the flotation recovery of pyrite in cyanide residues and the cyanide removal efficiency of cyanide residues.

Different methods, including acidification, chemical oxidation, and biological processes, have been employed to treat cyanide in wastewater and waste residues [6]. Cyanide recovery can be achieved using acidification, where the cyanide-containing system is acidified to pH of 2–3, which results in volatilization of hydrogen cyanide (HCN), which can then be recovered through absorption in an alkaline solution, such as NaOH or $Ca(OH)_2$ [7]. However, the acidification process often cannot destroy cyanide completely and requires secondary treatment. Although the biological process is environmentally friendly, there are disadvantages such as long processing time, high costs, and effectiveness limited to low cyanide concentrations [8]. In practical applications, chemical oxidation methods are extensively utilized, such as alkaline chlorination [9], hydrogen peroxide oxidation [10], and ozonation [11]. These methods effectively destroy free cyanides (CN^-) and weak acid-dissociable (WADs) metal complex cyanides but cannot efficiently remove stable strong acid-dissociable (SADs) complex cyanides, including iron–cyanide complexes [7]. The SO_2/air process, commonly

✉ Corresponding author: Hongying Yang E-mail: yanghy@smm.neu.edu.cn

known as the Inco process, which was developed by Inco Metals Company (Canada) in the 1980s, removes cyanide by the synergistic oxidation of SO_2 and oxygen under alkaline conditions (Eq. (1)) [7]. Because of the inconvenience of transporting SO_2 gas, solid forms such as soluble sulfite (Na_2SO_3) or metabisulfite ($Na_2S_2O_5$) can be utilized to supply the required SO_2 (as shown in Eqs. (2) and (3)) [12]. The Inco process is effective for both cyanide-containing solutions and slurries. An advantage of this process is that it can treat all forms of cyanide, including iron–cyanide complexes, making it one of the most widely used decyanation processes for gold cyanide residues in practical applications [13]. Pyrite is one of the main metallic minerals in cyanide residues. Therefore, investigating the cyanide leaching of pyrite, the process parameters, and the mechanism of pyrite cyanide residue decyanation is imperative, which can offer a theoretical foundation for the decyanation process of gold cyanide residues in actual production.

$$CN^- + SO_2 + O_2 + H_2O \rightarrow CNO^- + SO_4^{2-} + 2H^+ \quad (1)$$

$$CN^- + SO_3^{2-} + O_2 \rightarrow CNO^- + SO_4^{2-} \quad (2)$$

$$2CN^- + S_2O_5^{2-} + 2O_2 + H_2O \rightarrow 2CNO^- + 2SO_4^{2-} + 2H^+ \quad (3)$$

In this work, cyanidation of pyrite was performed to explore the interaction mechanism of cyanide with pyrite under different pH values, cyanide concentrations, and pyrite dosages. Pyrite was treated under actual cyanidation conditions for gold production, and the decyanation of the pyrite cyanide residue was performed by using the Na_2SO_3/air oxidation process. A response surface methodology (RSM) was employed to optimize the pH, SO_3^{2-} dosage, and air flow rate during the cyanide removal process. The mechanisms of cyanidation and decyanation of pyrite were determined by X-ray photoelectron spectroscopy (XPS) analysis of different pyrite samples.

2. Experimental

2.1. Materials and reagents

Industrial pyrite (Guangxi Province, China) containing 48.90wt% S and 45.85wt% Fe was used (Table 1). The mineral blocks were hand-selected, washed, and dried. The particle size of the pyrite powders was less than 74 μm by using a pulverizer (SJ1000-1, Jiangxi, China). Analytical NaOH (Damao, Tianjin, China) was used to adjust the pH. Analytical grade Na_2SO_3 (Damao, Tianjin, China) was used as the decyanation agent. Deionized water was used in all experiments.

Table 1. Chemical composition of the pyrite sample wt%

S	Fe	Si	Pb	Al	Zn	Others
48.90	45.85	1.86	1.05	0.81	0.75	0.78

2.2. Pyrite cyanidation

Ten grams of pyrite powder were added to sodium cyanide (NaCN) solutions with different initial cyanide (CN^-) concentrations. NaOH was added to maintain and stabilize the pH of the cyanidation system. After a certain reaction time, the slurry was filtered. The pyrite cyanide leaching residue was dried, and the cyanide concentration in the filtrate was determined to investigate the interaction of cyanide with pyrite.

2.3. Decyanation of the pyrite cyanide residue

The pyrite cyanide residue for decyanation tests was obtained by cyanidation of pyrite slurry (30wt% pyrite) under industrial production conditions of pH 11.5 and 0.1wt% NaCN for 24 h. Approximately 30 g of pyrite cyanide residues was added to deionized water in a 300 mL beaker to prepare the pyrite cyanide residue slurry (30wt% pyrite cyanide residue). The pH of the slurry was adjusted by NaOH. Decyanation tests were conducted by using the Na_2SO_3/air oxidation method, a traditional industrial cyanide removal method. Air was pumped into the slurry by an air compressor pump, and the air flow rate was controlled by a flowmeter. After a reaction time of 60 min, the slurry was filtered, and the concentration of total cyanide (TCN) in the decyanation residue was measured. To investigate the interaction of different factors during the cyanide removal process, a Box–Behnken design (BBD) with RSM was employed. Cyanide removal efficiency (η) was set as the response value and calculated using Eq. (4):

$$\eta = \frac{w_1 - w_2}{w_1} \times 100\% \quad (4)$$

where w_1 ($mg \cdot kg^{-1}$) and w_2 ($mg \cdot kg^{-1}$) are the concentration of TCN in the pyrite cyanide residue and pyrite decyanation residue, respectively.

2.4. Analytical methods

2.4.1. Determination of the cyanide concentrations

The TCN in solution and residue were collected by distillation (T/CGA 013-2019, China) [14], and the concentration of TCN was calculated with determining the free cyanide concentration (CN^-) in the distillate by using the silver nitrate titration method (HJ484-2009, China) [15]. Briefly, thymol phthalein and *p*-dimethylaminobenzylidene rhodanine were dissolved in acetone and used as indicators. 1 $mol \cdot L^{-1}$ NaOH solution was used to adjust the pH value of solution over 12, 3–5 drops of indicators were added, and the free cyanide was titrated with silver nitrate until the solution turned from black green to purplish red. Three parallel samples were performed, and the mean value was taken as the final result.

2.4.2. XPS analysis

XPS analysis (250Xi-type, Thermo Fisher Scientific, America) was performed to elucidate the mechanism of cyanidation and decyanation. Three samples were examined: pyrite (Sample A), pyrite cyanide residue (Sample B), and pyrite decyanation residue (Sample C). Each sample was vacuum-dried at 60°C before being placed on a stainless-steel bar and added to the fore vacuum chamber of the spectrometer. XPS tests were conducted with a monochromatic

Al Kα X-ray (photo energy of 1486.6 eV) operated at 30 keV and 150 W. High-resolution Fe 2p, S 2p, and N 1s spectra were collected at a pass energy of 20 eV. The C 1s peak at 284.6 eV was employed to calibrate the binding energy. The error of the binding energy data was ±0.2 eV. Data acquisition and processing were conducted with Thermo Avantage software. A schematic diagram of the experimental process in this study is illustrated in Fig. 1.

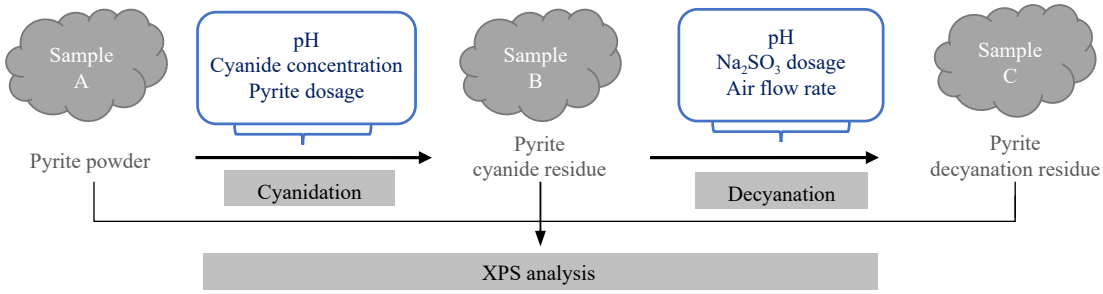

Fig. 1. Schematic diagram of the experimental process.

3. Results and discussion

3.1. Pyrite cyanidation

3.1.1. Effect of pH on pyrite cyanidation

The effect of pH on pyrite cyanidation was investigated by a series of experiments with different pH values, an initial cyanide concentration of 130 mg·L^{-1}, and a pyrite dosage of 5wt%. The results of the experiments are shown in Fig. 2(a), where C_0 and C_e are the cyanide concentration in the initial cyanide solution and the leaching solution after cyanidation, respectively. With the increasing initial pH of the cyanidation system, the interaction between CN^- and pyrite gradually strengthened. At pH above 13, approximately 70% of CN^- interacted with pyrite. It was found that the cyanidation of pyrite was nearly complete within 30 min, with the cyanide concentration in the leaching solution stabilizing after this duration. The rate constant for pyrite cyanidation within the initial 30 min was determined, and the experimental data fit the pseudo-second-order model closely. The correlation between the data and the model was supported by high correlation coefficients (R^2) in each case. The reaction kinetics for pyrite cyanidation can be calculated using Eq. (5):

$$-\frac{dC_e}{dt} = K_{app}C_e^2 \tag{5}$$

where t is the time, and K_{app} is the apparent rate constant. The linear graphs of $(1/C_e - 1/C_0)$ versus time were plotted, and K_{app} was determined from the slopes, as shown in Fig. 2(b). The increase in pH led to the increase in K_{app} because of the high degree of pyrite cyanidation.

The results demonstrate that pyrite in gold cyanide residues inevitably interacts with CN^- during the cyanidation process, especially under alkaline conditions. The high degree of cyanide interaction with pyrite resulted in high NaCN consumption during cyanidation, which negatively impacts the decyanation and flotation recovery of cyanide residues. Thus, pH should be optimized and controlled not be too high to weaken the interaction of cyanide with pyrite during the cyanidation process.

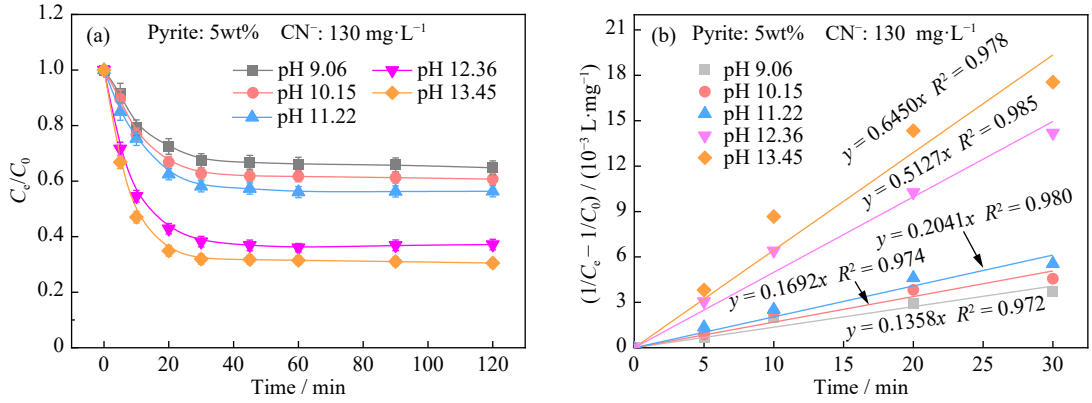

Fig. 2. (a) Change in CN^- concentration and (b) corresponding validation of the pseudo-second-order kinetics (solid line is fiting result) for the cyanidation of pyrite with different pH values.

3.1.2. Effect of cyanide concentration on pyrite cyanidation

To explore the effect of cyanide concentration on pyrite cyanidation (Fig. 3(a)), pyrite cyanidation experiments with pH 12.0, pyrite dosage of 5wt%, and different initial cyanide concentrations were performed. A gradual improvement in the proportion of cyanide interacting with pyrite was observed as the cyanide concentration increased. Pyrite with 5wt% dosage could interact with over 90% of free CN^- when the concentrations of the cyanide solution were 260 and 520 mg·L^{-1}. High cyanide concentrations can have an inhibitory effect on the cyanidation of gold ores and the subsequent recovery of mineral flotation of cyanide residues [3]. Thus, it is imperative to choose a suitable cyanide concentration during the cyanidation process.

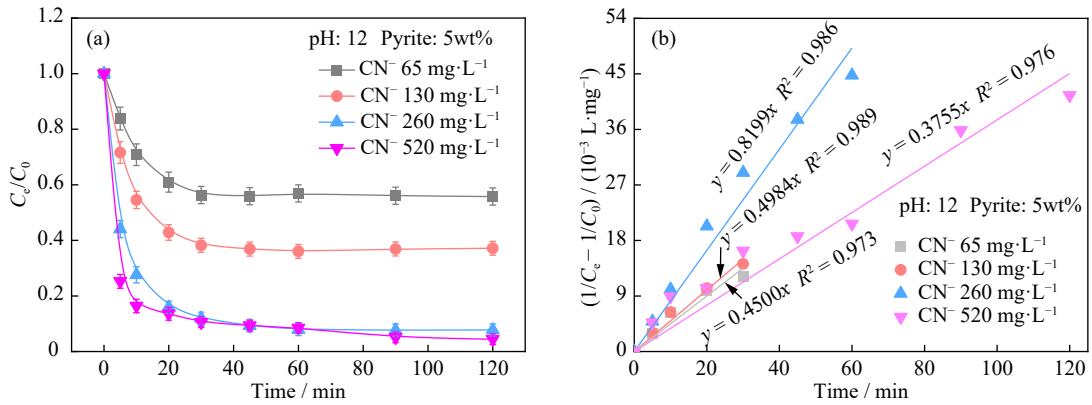

Fig. 3. (a) Change in CN^- concentration and (b) corresponding validation of the pseudo-second-order kinetics for the cyanidation of pyrite with different initial CN^- concentrations.

From Fig. 3(b), it was worth noting that the reaction rate constant increased gradually with increasing cyanide concentration from 65 to 260 mg·L^{-1}; however, at an initial cyanide concentration of 520 mg·L^{-1}, the reaction rate constant of pyrite cyanidation decreased to its lowest point.

Fig. 4 presents the concentration of Fe element in the leaching solution after pyrite cyanidation with different initial CN^- concentrations and pH. It is worth noting that, even in the system without cyanide, a certain amount of Fe element was generated through Eqs. (6) and (7) [16]. In an aqueous solution, pyrite can be first oxidized to Fe^{2+}, which can be further oxidized to Fe^{3+} by O_2 after dissolution. In a cyanide-containing system, Fe ions and CN^- interact to form iron–cyanide complexes (such as $Fe(CN)_6^{4-}$ and $Fe(CN)_6^{3-}$), adsorbed on the pyrite surface, or combine to obtain iron–cyanide precipitates that are removed from the solution (Eqs. (8) and (9)) [17]. This process led to a decrease in concentration of Fe element in the leaching solution. The accumulation of adsorbed substances and precipitates on the pyrite surface hindered further reactions, which was reflected in the decline in the cyanidation rate observed at a high initial CN^- concentration of 520 mg·L^{-1}. In Fig. 4(b), the concentration of Fe element in the leaching solution gradually decreased with the increase of pH in the cyanidation system. The main reason for this phenomenon may be the formation of iron hydroxide precipitates ($Fe(OH)_2$ and $Fe(OH)_3$) under high pH conditions [18]. The precipitates enveloped on the surface of the pyrite would hinder the leaching of Fe.

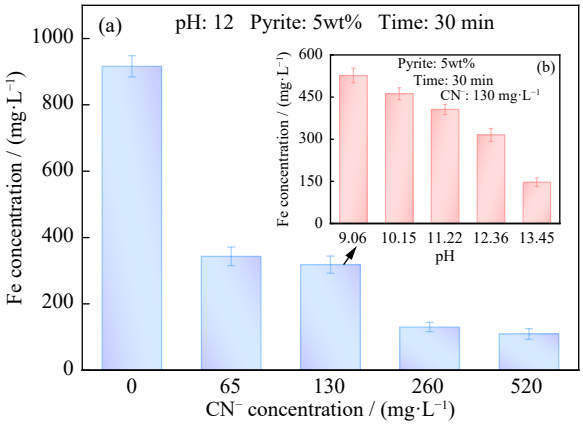

Fig. 4. Concentration of Fe in the leaching solution after pyrite cyanidation with different (a) initial CN^- concentrations and (b) pH values.

$$FeS_2 + 7/2O_2(aq) + H_2O \rightarrow Fe^{2+} + 2SO_4^{2-} + 2H^+ \quad (6)$$

$$2Fe^{2+} + 1/2O_2(aq) + 2H^+ \rightarrow 2Fe^{3+} + H_2O \quad (7)$$

$$4Fe^{3+} + 3Fe(CN)_6^{4-} \rightarrow Fe_4[Fe(CN)_6]_3\downarrow \quad (8)$$

$$2Fe^{2+} + Fe(CN)_6^{4-} \rightarrow Fe_2[Fe(CN)_6]\downarrow \quad (9)$$

3.1.3. Effect of pyrite dosage on pyrite cyanidation

Under the conditions of 130 mg·L^{-1} CN^- concentration and pH = 12.0, the effect of pyrite dosage on pyrite cyanidation was observed (Fig. 5). The results revealed that as the pyrite dosage increased from 5wt% to 25wt%, the interaction of CN^- with pyrite increased from 62.9% to 86.1%. Further increasing the pyrite dosage to 40wt% resulted in a proportion of 88.4%, with no significant increase compared with that of the 25wt% pyrite dosage. The increase in pyrite dosage not only led to increased cyanide consumption but also sped up the cyanidation rate.

The results of the pyrite cyanidation tests demonstrate that pH conditions, initial cyanide concentration, and pyrite dosage significantly affect the interaction of cyanide with pyrite. If a strong interaction takes place during the cyanidation of gold ore, it results in the generation of a substantial quantity of iron–cyanide complexes. Cyanide complexes not only affect gold recovery but also produce gold cyanide residues with high cyanide concentrations that are difficult to treat and seriously inhibit the subsequent flotation recovery of other valuable minerals in the cyanide residues [19]. To prevent this issue and acquire high gold recovery, the cyanidation system parameters should be carefully controlled, which are a slurry concentration of 30wt%–40wt%, pH of 11.0–12.0, NaCN dosage of 0.1wt%–0.5wt%, and leaching time of 24–48 h, in practical cyanidation processes.

3.2. Decyanation of the pyrite cyanide residue

In this study, the pyrite cyanide residue was produced by cyanidation under the conditions of 30wt% pyrite slurry at pH 11.5 with 0.1wt% NaCN for 24 h. The TCN concentration in the obtained pyrite cyanide residue was 923 mg·kg^{-1}.

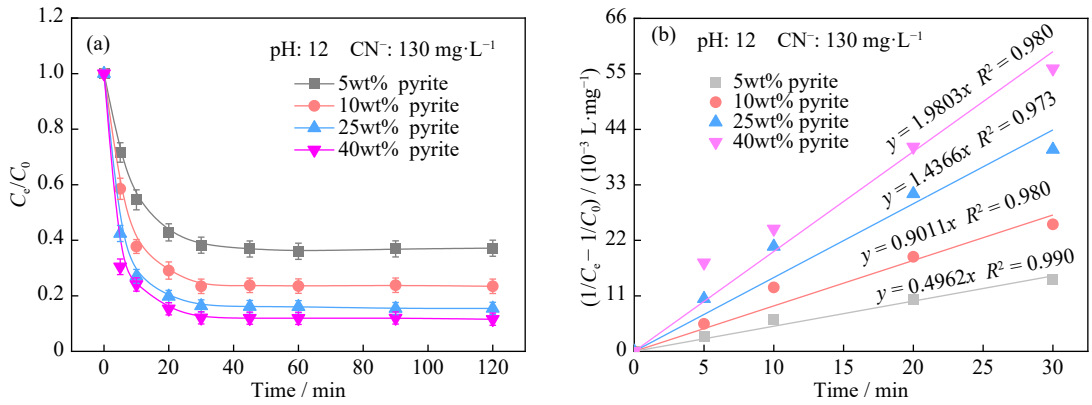

Fig. 5. (a) Change in CN^- concentration and (b) corresponding validation of the pseudo-second-order kinetics for the cyanidation of pyrite with different pyrite dosages.

To prevent the release of HCN gas during the decyanation process, blank control experiments were performed under different pH conditions without the addition of decyanation agents. The escaped HCN gas was subsequently absorbed by 100 mL of 1 mol·L^{-1} NaOH solution. All decyanation tests were performed at a slurry with pyrite cyanide residue content of 30wt% and reaction time of 60 min. Fig. 6 illustrates the change in the cyanide content in residues and the NaOH absorption solution. At pH below 9, the TCN content within the cyanide residue decreased with the decrease of pH due to the evolution of HCN gas. At pH above 9, the TCN content in the residue did not decrease obviously because only a small portion of the cyanide eluted into the liquid phase. Therefore, an oxidizing agent was required to remove the cyanide, and the initial pH value of the slurry should be adjusted over 9 to avoid the evolution of HCN during the decyanation process.

To examine the cyanide removal of pyrite cyanide residue by Na_2SO_3/air oxidation, a series of 17 experiments for the RSM were conducted to optimize the pH value, SO_3^{2-} dosage, and air flow rate, with the cyanide removal efficiency as the response value. The experimental design and the results of cyanide removal are summarized in Table 2. After data fitting and regression analysis, the following polynomial equation (Eq. (10)) was obtained for cyanide removal efficiency:

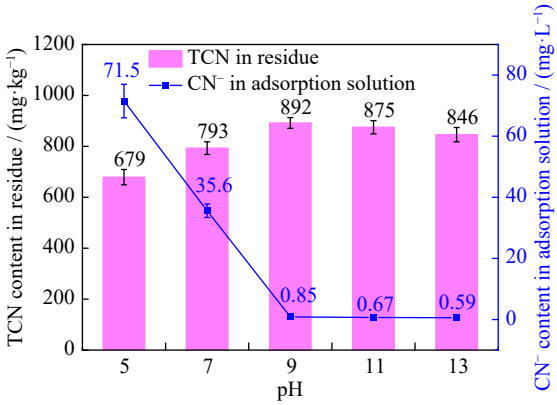

Fig. 6. Cyanide content in pyrite cyanide residue and absorption solution at different pH values.

Table 2. Experimental design and results of cyanide removal

Number	Design			Response, η / %
	pH	SO_3^{2-} dosage / (mg·g^{-1})	Air flow rate / (L·min^{-1})	
1	11	20	1.5	83.3
2	13	20	1.0	68.1
3	11	30	2.0	79.4
4	9	10	1.5	58.9
5	9	30	1.5	62.2
6	13	20	2.0	68.5
7	11	20	1.5	82.6
8	11	10	1.0	76.1
9	11	20	1.5	82.9
10	13	10	1.5	63.2
11	13	30	1.5	67.6
12	9	20	1.0	66.1
13	11	30	1.0	80.3
14	11	10	2.0	75.9
15	11	20	1.5	82.7
16	11	20	1.5	83.5
17	9	20	2.0	66.3

$$\eta = -422.3 + 86.04A + 2.044B - 7.225C + 0.01375AB + 0.005AC - 0.035BC - 3.887A^2 - 0.0487B^2 - 2.4C^2 \quad (10)$$

where η is the cyanide removal efficiency (%), A is the initial pH of the pyrite cyanide residue slurry, B is the dosage of SO_3^{2-} for per gram pyrite (mg·g^{-1}), and C is the air flow rate (L·min^{-1}). The results of the variance regression analysis are presented in Table 3, showing that the model for the cyanide removal efficiency was significant (model F-value = 149.85, P-value < 0.0001) [9]. The "Lack of fit P-value" was 0.1975 (>0.1), showing that the lack of fit due to noise was not significant. The r^2_{adj} of 0.9882 suggested that there was only a 3% chance that the cyanide removal efficiency could not be explained by this model. The coefficient of determination (r^2) of the model was 0.9948, which verified that there was a high degree of fit between the measured and predicted values of the cyanide removal efficiency. A model was considered adequate with an "Adeq Precision" of over 4, and it reached

Table 3. Analysis of the variance regression model for the cyanide removal efficiency

Source	Sum of square	df	Mean square	*F*-value	*P*-value
Model	1221.99	9	135.78	149.85	<0.0001
pH	24.15	1	24.15	26.65	0.0013
SO_3^{2-} dosage	29.64	1	29.64	32.72	0.0007
Air flow	0.0313	1	0.0313	0.0345	0.8579
AB	0.3025	1	0.3025	0.3339	0.5815
AC	0.0100	1	0.0100	0.0110	0.9193
BC	0.1225	1	0.1225	0.1352	0.7240
A^2	1018.12	1	1018.12	1123.66	<0.0001
B^2	100.07	1	100.07	110.44	<0.0001
C^2	1.52	1	1.52	1.67	0.2369
Residual	6.34	7	0.9061		
Lack of fit	4.14	3	1.38	2.51	0.1975
Pure error	2.20	4	0.5500		
Cor total	1228.33	16			

Note: df—degree of freedom; Cor—correlation.

32.6173 with this model. The experimental results had high repeatability with a low value (1.29%) of the coefficient of variance (C.V.) [20]. The results of the analysis of variance regression corroborate the reliable use of the model to predict the actual cyanide removal efficiency.

Response surface and contour plots of cyanide removal are presented in Fig. 7. The effects of these three factors and their interactions were determined. The steeper the surface in the stereogram of the response surface, the more significant the influence of the corresponding factor on the response value [21]. If there is a perfect interaction between independent variables, elliptical contours can be obtained [22]. From Fig. 7(a), the interaction between pH and SO_3^{2-} dosage was the most apparent. The contours in Fig. 7(b) and (c) were not perfectly elliptical, showing fewer interactions between air flow and other factors associated with the response surface. The effect of air flow range 1–2 L·min^{-1} on cyanide removal efficiency was little. With increasing pH from 9 to 13, the cyanide removal efficiency initially increased and subsequently decreased, which is consistent with the effect of SO_3^{2-} dosage of 10–30 mg·g^{-1}. The highest efficiency was obtained under medium alkalinity (pH 10–12) and medium SO_3^{2-} dosage (about 15–25 mg·g^{-1}). Based on the RSM model, the optimal cyanide removal efficiency could be obtained under the conditions of pH = 11.2, SO_3^{2-} dosage = 22 mg·g^{-1}, and air flow rate = 1.46 L·min^{-1}, leading to an efficiency of 83.9% in the actual experiment.

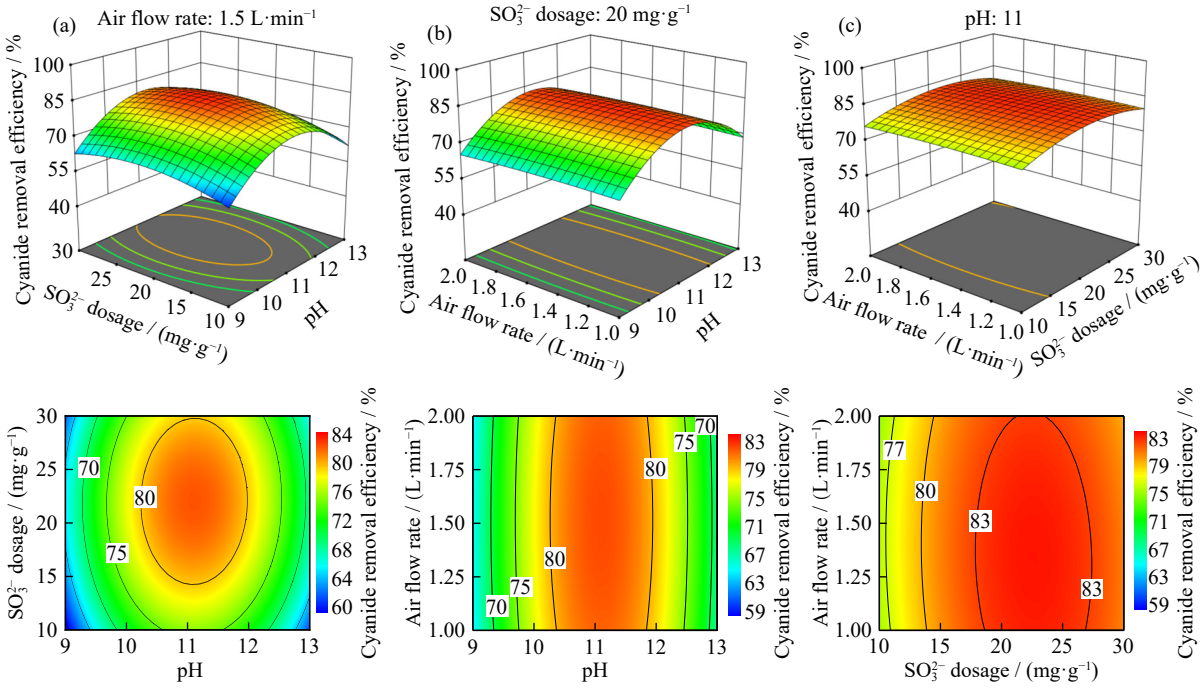

Fig. 7. Response surface and contour plots: (a) pH and SO_3^{2-} dosage; (b) pH and air flow; (c) SO_3^{2-} dosage and air flow.

3.3. XPS analysis

To examine the alterations in the forms of key elements present during the cyanidation and decyanation of pyrite, XPS analysis of pyrite containing samples was conducted. The survey spectra covering a binding energy range of 1350–0 eV of different pyrite samples are presented in Fig. 8(a). The XPS spectrum of the pyrite containing samples showed peaks at approximately 711.05 and 162.33 eV, which are attributed to the Fe 2p and S 2p signals, respectively [23]. Moreover, C 1s and N 1s were detected on the sample surfaces. Comparison of atomic concentrations of C 1s and N 1s after the cyanidation and decyanation process is shown in Fig. 8(b). It was shown that 18.08at% C 1s and 0.95at% N 1s were present on the surface of pure pyrite (Sample A) caused by pollution. After cyanidation, the concentrations of C 1s and N 1s increased to 30.16at% and 6.02at%, respectively. This increase noted that cyanide was absorbed on the pyrite surface, increasing the difficulty of decyanation. Comparing the pyrite cyanide residue (Sample B) with the pyrite decyanation residue (Sample C, which was obtained under the optimized conditions of pH 11.2, dosage of 22 $mg \cdot g^{-1}$, and air flow rate of 1.46 $L \cdot min^{-1}$), the atomic concentrations of both C 1s and N 1s decreased after decyanation by Na_2SO_3/air oxidation. N 1s was not detected on the surface of Sample C, indicating the effective removal of cyanide by Na_2SO_3/air oxidation.

Fig. 9 presents the XPS spectra (Fe 2p, S 2p, and N 1s) of the three pyrite containing samples. The composition of chemical states on the surface of the samples (Fe 2p and S 2p) are summarized in Table 4. Five peaks appeared in the Fe 2p spectrum of the original pyrite (Sample A), corresponding to FeS_2 (706.05 eV, 718.91 eV), Fe(II) (710.10 eV, 722.86 eV), and Fe(III) (713.72 eV) [24–25]. With a content of 6.62at%, Fe(III) may be due to oxidation pollution during storage and testing. In the Fe 2p spectrum of pyrite after cyanidation (Sample B), the peak at 726.66 eV was attributed to Fe(III) [26]. The occurrence of a new peak led to an increased Fe(III) content and decreased FeS_2 and Fe(II) contents, showing that pyrite oxidation took place during the cyanidation process. In the Fe 2p spectrum of Sample C, another peak representing Fe(III) (713.09 eV) emerged, and the Fe(III) content increased continuously [27]. During the cyanide removal process by Na_2SO_3/air oxidation, oxygen intake triggered the rapid oxidation of pyrite in a short time.

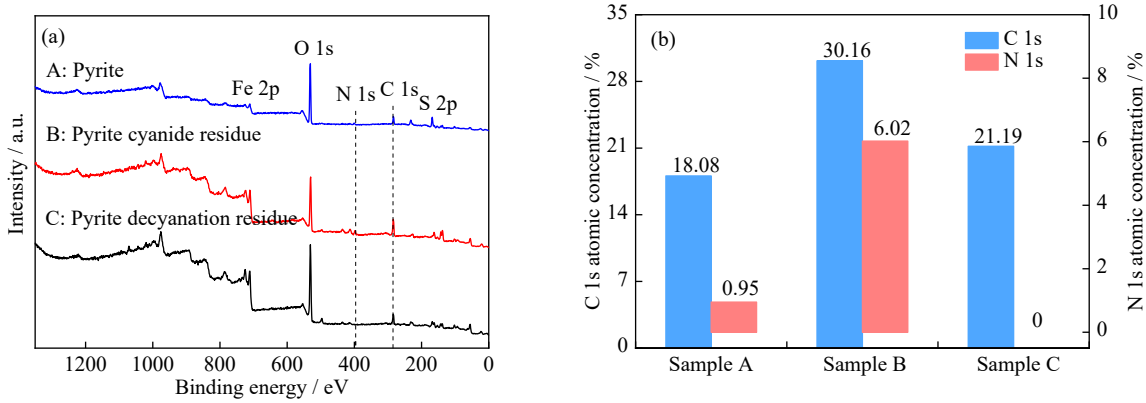

Fig. 8. (a) XPS survey spectra and (b) atomic concentrations of C 1s and N 1s on the surfaces of three pyrite containing samples.

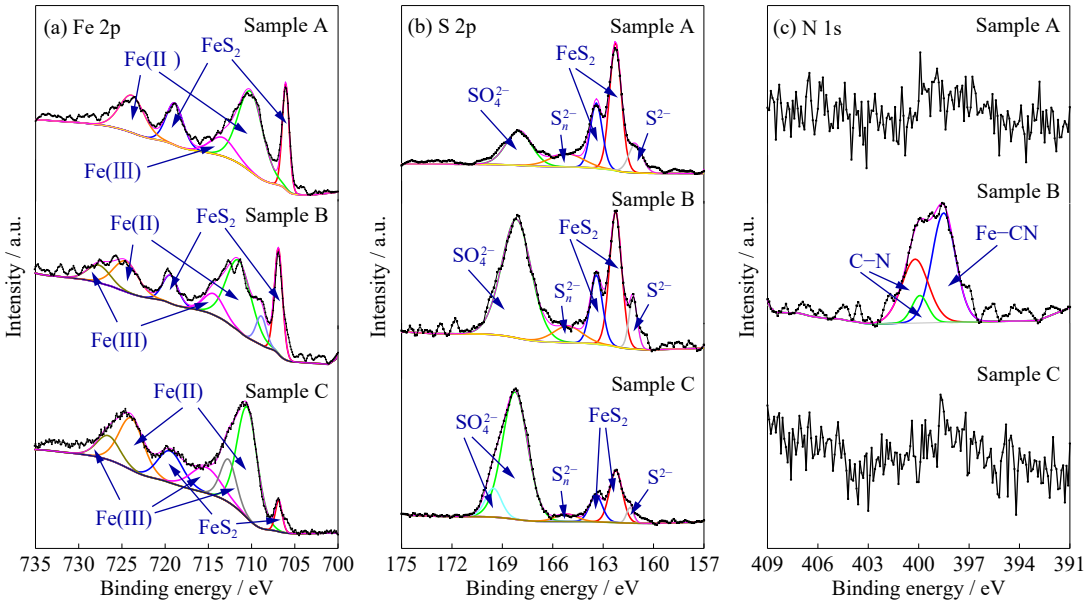

Fig. 9. Fe 2p (a), S 2p (b), and N 1s (c) spectra of three pyrite containing samples.

Table 4. Atomic concentrations of chemical states (Fe and S) on the surfaces of samples %

Sample	Fe 2p			S 2p			
	FeS_2	Fe(II)	Fe(III)	FeS_2 (S_2^{2-})	SO_4^{2-}	S_n^{2-}	S^{2-}
A—pyrite	32.71	60.67	6.62	56.98	22.26	10.95	9.81
B—pyrite cyanide residue	26.24	56.74	17.02	36.04	50.76	7.11	6.09
C—pyrite decyanation residue	22.79	50.52	26.69	20.78	74.02	3.25	1.95

Fig. 9(b) shows that the S 2p peaks of the pyrite sample were ascribed to four species: FeS_2/S_2^{2-} (162.26 eV, 163.40 eV), SO_4^{2-} (168.02 eV), S_n^{2-} (165.17 eV), and S^{2-} (161.08 eV) [24,28]. To stabilize the surface state and attain charge neutrality, the unstable S^- monomer may reduce to the most stable monosulfide (S^{2-}), as presented in Eq. (11). The S^- surface species may acquire more electrons from adjacent Fe^{2+} ions to generate surface Fe^{3+} ions [29]. The apparent increase in SO_4^{2-} content on the surface of Sample B was ascribed to the oxidation of sulfide, especially S^- (Eq. (6)). Combined with the fitting results of the Fe 2p spectra, it was indicated that the SO_4^{2-} species on the surface of pyrite mainly exist as $FeSO_4$ after the cyanidation process. On the surface of Sample C, the sulfide content decreased significantly, and the predominant form of S 2p was SO_4^{2-}, with a content of 74.02at%. A peak with higher binding energy (169.13 eV) was observed and related to $Fe_2(SO_4)_3$ [30], demonstrating that side reactions, including pyrite oxidation, were inevitable during the cyanide removal process. This accounts for the necessity of exceeding the theoretically calculated SO_3^{2-} dosage for effective cyanide removal.

$$Fe^{2+}_{surface} + S^{-}_{surface} \rightarrow Fe^{3+}_{surface} + S^{2-}_{surface} \quad (11)$$

The N 1s spectra of the pyrite samples are shown in Fig. 9(c). The results indicated that the cyanides adsorbed on the pyrite surface after cyanidation primarily existed as Fe–CN and C–N, with Fe–CN being the majority at 62.64wt% [27]. Because the main form of Fe 2p on the surface of Sample B was Fe(II), it was speculated that the iron–cyanide complex produced during cyanidation was mainly $Fe(CN)_6^{4-}$. Compared with other metal complex cyanides (such as Cu–CN, Zn–CN), Fe–CN has greater stability and stronger adsorption on mineral surfaces, resulting in difficulty in cyanide removal of pyrite cyanide residues [3]. However, little cyanide was observed on the surface of Sample C, indicating that the cyanides (including iron–cyanide complexes) on the pyrite surface could be removed by Na_2SO_3/air oxidation. Cyanides were oxidized by reactive oxygen ([O]) generated from the synergistic reaction between SO_3^{2-} and O_2, as shown in Eqs. (12) and (13) [31]. During the cyanide removal process of pyrite, [O] also promoted pyrite oxidation, giving rise to the production of Fe(III) and SO_4^{2-}. Pyrite oxidation promoted the formation of Fe and S vacancies on the pyrite surface, thereby decreasing its adsorption capacity [32]. Cyanides adsorbed on the pyrite surface were displaced by other ions produced during the cyanide removal process. The displaced cyanides were then transferred into the solution and removed from the cyanide residue at the end. This is one reason for the presence of cyanide in the filtrate after the decyanation process, and another one is the prior oxidation of pyrite, causing the cyanide to be transferred into the solution without being completely oxidized.

$$SO_3^{2-} + O_2 \rightarrow SO_4^{2-} + [O] \quad (12)$$

$$CN^- + [O] \rightarrow CNO^- \quad (13)$$

The mechanisms of the cyanidation and decyanation processes of pyrite were elucidated by XPS analysis, as shown in the illustration in Fig. 10. During the cyanidation process, pyrite was oxidized to produce Fe(III) and $FeSO_4$. The cyanides adsorbed on the pyrite surface were found to exist mainly as CN^- and Fe–CN, with $Fe(CN)_6^{4-}$ being the predominant species. During the decyanation of the pyrite cyanide residue by Na_2SO_3/air oxidation, air intake triggered the effective removal of cyanide. The improved pyrite oxidation promoted the desorption of cyanides and the transfer of cyanide from the pyrite surface to the liquid phase. It is worth noting that the results in Section 3.2 exhibited that air flow rate had a limited impact on cyanide removal efficiency but significantly influenced the oxidation of pyrite as the main side reaction. During the decyanation process of gold cyanide residues in industry, some Fe ions entered the solution because of pyrite oxidation, which affected the recycling and detoxification of the cyanide-containing solution. The oxidation of pyrite during the decyanation process also caused the loss of valuable minerals in the cyanide residues and influenced the subsequent flotation recovery. Thus, the process conditions of Na_2SO_3/air oxidation decyanation must be controlled, and appropriate air flow rate should be chosen to ensure the effective removal of cyanide while weakening the pyrite oxidation as much as possible.

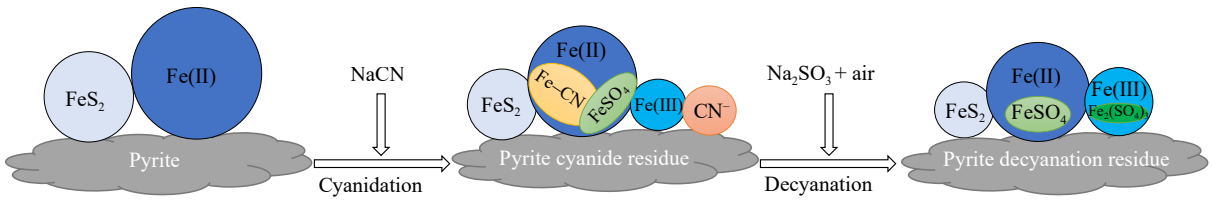

Fig. 10. Schematic of cyanidation and decyanation of pyrite.

4. Conclusion

In this work, the interaction of cyanide with pyrite during the cyanidation process of pyrite and the decyanation process of pyrite cyanide residue were examined. During the cyanidation process of pyrite, the pH of system, cyanide concentration, and pyrite dosage were positively correlated with the degree of pyrite–cyanide interaction. Kinetic analysis revealed that the cyanidation of pyrite was pseudo-second-order with respect to cyanide. The results of the decyanation process of pyrite cyanide residues by Na_2SO_3/air oxidation demonstrated that the effect of pH and SO_3^{2-} dosage on cyanide removal efficiency was significant, whereas that of air flow rate was little. The cyanide removal efficiency was 83.9% under the optimized conditions of pH 11.2, SO_3^{2-} dosage of 22 $mg \cdot g^{-1}$, and air flow rate of 1.46 $L \cdot min^{-1}$. XPS analysis elucidated the mechanisms of cyanidation and decyanation of pyrite. After the cyanidation process, the oxidation of pyrite led to the production of Fe(III) and $FeSO_4$, and the cyanide adsorbed on the surface of pyrite existed mainly as CN^- and $Fe(CN)_6^{4-}$. During the decyanation process of the pyrite cyanide residue, cyanides were effectively removed by the synergy action of SO_3^{2-} and O_2. Improved pyrite oxidation promoted the desorption of cyanides and the transfer of cyanide from the pyrite surface to the solution by added air. The air flow rate had little effect on the cyanide removal efficiency but affected the oxidation of pyrite during the decyanation process. This work has considerable significance for the cyanidation of sulfide gold ores and the removal of cyanide in gold cyanide residues.

Acknowledgements

This word was financially supported by the National Natural Science Foundation of China (No. 52274348), the Major projects for the "Revealed Top" Science and Technology of Liaoning Province, China (No. 2022JH1/10400024), and the National Key Research and Development Program of China (No. 2018YFC1902002).

Conflict of Interest

The authors declare no competing financial interest.

References

[1] Z.W. Liu, X.Y. Guo, Q.H. Tian, and L. Zhang, A systematic review of gold extraction: Fundamentals, advancements, and challenges toward alternative lixiviants, *J. Hazard. Mater.*, 440(2022), art. No. 129778.

[2] Y. Xu, W.S. Li, Q.F. Huang, *et al*., Long-term degradation characteristics of cyanide in closed monofills and its effects on the environment and human health: Evidence from nine landfill sites in northern China, *Sci. Total Environ.*, 839(2022), art. No. 156269.

[3] B. Guo, Y.J. Peng, and R. Espinosa-Gomez, Cyanide chemistry and its effect on mineral flotation, *Miner. Eng.*, 66-68(2014), p. 25.

[4] W.W. Han, H.Y. Yang, and L.L. Tong, Cyanide removal for ultrafine gold cyanide residues by chemical oxidation methods, *Trans. Nonferrous Met. Soc. China*, 32(2022), No. 12, p. 4129.

[5] C.H. Zhao, D.W. Huang, J.H. Chen, Y.Q. Li, Y. Chen, and W.Z. Li, The interaction of cyanide with pyrite, marcasite and pyrrhotite, *Miner. Eng.*, 95(2016), p. 131.

[6] C. Anning, J.X. Wang, P. Chen, I. Batmunkh, and X.J. Lyu, Determination and detoxification of cyanide in gold mine tailings: A review, *Waste Manage. Res.*, 37(2019), No. 11, p. 1117.

[7] N. Kuyucak and A. Akcil, Cyanide and removal options from effluents in gold mining and metallurgical processes, *Miner. Eng.*, 50-51(2013), p. 13.

[8] A. Akcil, Destruction of cyanide in gold mill effluents: Biological versus chemical treatments, *Biotechnol. Adv.*, 21(2003), No. 6, p. 501.

[9] Q. Xiong, S.J. Jiang, R. Fang, *et al*., An environmental-friendly approach to remove cyanide in gold smelting pulp by chlorination aided and corncob biochar: Performance and mechanisms, *J. Hazard. Mater.*, 408(2021), art. No. 124465.

[10] M. Kitis, A. Akcil, E. Karakaya, and N.O. Yigit, Destruction of cyanide by hydrogen peroxide in tailings slurries from low bearing sulphidic gold ores, *Miner. Eng.*, 18(2005), No. 3, p. 353.

[11] F. Barriga-Ordonez, F. Nava-Alonso, and A. Uribe-Salas, Cyanide oxidation by ozone in a steady-state flow bubble column, *Miner. Eng.*, 19(2006), No. 2, p. 117.

[12] D. Hewitt, P. Breuer, and C. Jeffery, Cyanide detoxification of gold cyanidation tails and process streams, *Miner. Process. Extr. Metall.*, 121(2012), No. 4, p. 228.

[13] P.L. Breuer and D.M. Hewitt, INCO Cyanide destruction insights from plant reviews and laboratory evaluations, *Miner. Process. Extr. Metall.*, 129(2020), No. 1, p. 104.

[14] China Gold Association, T/CGA 013–2019: *Method for Chemical Analysis of Cyanide Leaching Residue in Gold Industry—Determination of Cyanide Titration and Spectrophotometry Method*, 2019.

[15] Ministry of Environmental Protection of the People's Republic of China, HJ 484–2009: *Water Quality—Determination of Cyanide—Volumetric and Spectrophotometry Method*, 2009.

[16] Y.B. Li, Y. Peng, Z.L. Wei, X. Yang, and A.R. Gerson, Crystal face-dependent pyrite oxidation: An electrochemical study, *Appl. Surf. Sci.*, 619(2023), art. No. 156687.

[17] B. Guo, Y.J. Peng, and G. Parker, Electrochemical and spectroscopic studies of pyrite–cyanide interactions in relation to the depression of pyrite flotation, *Miner. Eng.*, 92(2016), p. 78.

[18] A.M. Raichur, X.H. Wang, and B.K. Parekh, Quantifying pyrite surface oxidation kinetics by contact angle measurements, *Colloids Surf. A*: *Physicochem. Eng. Aspects*, 167(2000), No. 3, p. 245.

[19] X.M. Qiu, H.Y. Yang, G.B. Chen, L.L. Tong, Z.N. Jin, and Q. Zhang, Interface behavior of chalcopyrite during flotation from cyanide tailings, *Int. J. Miner. Metall. Mater.*, 29(2022), No. 3, p. 439.

[20] R. Fattahi, M. Lashkarbolooki, R. Abedini, and H. Younesi, Analysis of the interfacial tension of cationic imidazolium-based ionic liquid, twin-branched tailed anionic surfactant, and a non-ionic emulsifier in the presence of SiO_2 nanoparticle and amphiphilic oleic components using response surface method, *J. Mol. Liq.*, 381(2023), art. No. 121799.

[21] H.H. Xue, J.Y. Li, G.B. Zhang, M. Li, B.S. Liu, and C.L. Kang, Hydroxyl radical dominated ibuprofen degradation by UV/percarbonate process: Response surface methodology optimization, toxicity, and cost evaluation, *Chemosphere*, 329(2023), art. No. 138681.

[22] R.V. Muralidhar, R.R. Chirumamila, R. Marchant, and P. Nigam, A response surface approach for the comparison of lipase production by *Candida cylindracea* using two different carbon sources, *Biochem. Eng. J.*, 9(2001), No. 1, p. 17.

[23] Q.F. Zhao, H.Y. Yang, L.L. Tong, R.P. Jin, and P.C. Ma, Understanding the effect of grinding media on the adsorption mechanism of cyanide to chalcopyrite surface by ToF–SIMS, XPS, contact angle, zeta potential and flotation, *Colloids Surf. A: Physicochem. Eng. Aspects*, 644(2022), art. No. 128799.

[24] Y.F. Mu, L.Q. Li, and Y.J. Peng, Surface properties of fractured and polished pyrite in relation to flotation, *Miner. Eng.*, 101(2017), p. 10.

[25] X.L. Zhang, Y.X. Han, P. Gao, Y.J. Li, and Y.S. Sun, Effects of particle size and ferric hydroxo complex produced by different grinding media on the flotation kinetics of pyrite, *Powder Technol.*, 360(2020), p. 1028.

[26] M. Cheng, Y. Liu, D.L. Huang, *et al*., Prussian blue analogue derived magnetic Cu–Fe oxide as a recyclable photo-Fenton catalyst for the efficient removal of sulfamethazine at near neutral pH values, *Chem. Eng. J.*, 362(2019), p. 865.

[27] Q.M. Nie, M.Y. Wang, T.S. Qiu, and X.H. Qiu, Density functional theory and XPS studies of the adsorption of cyanide on chalcopyrite surfaces, *ACS Omega*, 5(2020), No. 36, p. 22778.

[28] G. Han, S.M. Wen, H. Wang, and Q.C. Feng, Selective adsorption mechanism of salicylic acid on pyrite surfaces and its application in flotation separation of chalcopyrite from pyrite, *Sep. Purif. Technol.*, 240(2020), art. No. 116650.

[29] M. Ejtemaei and A.V. Nguyen, Characterisation of sphalerite and pyrite surfaces activated by copper sulphate, *Miner. Eng.*, 100(2017), p. 223.

[30] Y.F. Cai, Y.G. Pan, J.Y. Xue, Q.F. Sun, G.Z. Su, and X. Li, Comparative XPS study between experimentally and naturally weathered pyrites, *Appl. Surf. Sci.*, 255(2009), No. 21, p. 8750.

[31] S. Qiu, Z.P. Guo, Q. Zheng, and B. Yan, Treatment of cyanide tailing slurry by $Na_2S_2O_5$–air method, *Nonferrous Met. Extr. Metal.*, 12(2015), p. 59.

[32] Y.B. Tu, P.W. Han, L.Q. Wei, *et al*., Removal of cyanide adsorbed on pyrite by H_2O_2 oxidation under alkaline conditions, *J. Environ. Sci.*, 78(2019), p. 287.